Effect of Annealing on the Crystal Structure and Microstructure of Pr Doped ZrO_2–Y_2O_3 Nanocrystals

E. Werner-Malento[a,*], W. Paszkowicz[a], J.D. Fidelus[b], M. Godlewski[a,c]

and S. Yatsunenko[a]

[a]Institute of Physics, Polish Academy of Sciences, al. Lotników 32/46, 02-668 Warsaw, Poland

[b]Institute of High Pressure Physics, Polish Academy of Sciences, Sokołowska 29/37, 01-142 Warsaw, Poland

[c]Department of Mathematics and Natural Sciences, College of Science, Cardinal S. Wyszyński University

Warsaw, Poland

Rare-earth doped nanocrystalline yttria-stabilized zirconia (YSZ, ZrO_2–Y_2O_3) is, recently, a subject of studies because of its luminescent properties. The luminescence may be strongly influenced by the crystal structure and microstructure of the material. In this work, the X-ray diffraction study for Pr doped YSZ nanocrystals is presented. The phase composition dependence on the Y_2O_3 content and on heat treatment conditions is quantitatively determined using the Rietveld method and the similarities and differences between the present data for doped samples and earlier reported data for undoped material are discussed. A formation of high symmetry phases (cubic and tetragonal) is observed for high yttria content in agreement with general tendencies observed in literature for undoped samples.

PACS numbers: 61.46.−w, 61.66.Fn, 81.40.−z

1. Introduction

Rare-earth (RE) doped nanocrystalline yttria-stabilized zirconia (YSZ, ZrO_2–Y_2O_3) is, recently, a subject of studies because of its physical properties (e.g. luminescence, hardness, chemical inertness) and various potential applications. YSZ exhibits a high-temperature stability, wear and corrosion resistance, and superionic conductivity at high temperature. The material is mostly used in jet engines, to determine oxygen content in exhaust gases, to measure pH in high temperature water, as membranes for high temperature solid oxide fuel cell, as a component of waveguides and laser mirrors, and optical filters, as well as for electrolytes or insulators in microelectronic devices. A special interest is connected with nanosized YSZ, for which synthesis routes have been developed (see a brief review by Bokhimi et al. [1]). One of properties of RE doped YSZ is the luminescence reported e.g. for RE = Eu [2], RE = Ho [3], RE = Dy [4], and RE = Pr [5]. The luminescence may be strongly influenced by the crystal structure and microstructure of the material. It has been observed that for nanosized material the efficiency of RE photoluminescence in ZrO_2 system is enhanced [5–8].

For undoped zirconia, ZrO_2, several polymorphs are known: (i) monoclinic (M) zirconia [9] of baddeleyite

type (space group $P2_1/a$, no. 14), (ii) tetragonal (T) zirconia [10] (space group $P4_2/nmc$, no. 137), (iii) and cubic (C) zirconia [11] of fluorite type (space group $Fm3m$, no. 225), a high temperature polymorph. The M–T transformation is observed at about 1170 °C, the T–C transition at about 2350 °C, and the melting point at 2715 °C. At high pressure, the monoclinic ZrO_2 transforms to orthorhombic phases (OrthoI: space group $Pbca$, OrthoII: space group $Pnma$) [12]. Annealing of bulk monoclinic zirconia, in agreement with the phase diagram (see e.g. Ref. [12]), leads to transformation to higher symmetry (T or C) phases. Both high-temperature polymorphs exhibit properties being advantageous for specific applications. Formation of high-symmetry phases is facilitated in the nanocrystalline materials as compared to systems with bulk (micron-size) material. A similar result can be obtained for thin films (see e.g. Ref. [13]).

In general, to get such high-symmetry phases, the stabilising effect of (i) various additives (not only yttria) or (ii) reduced crystallite size can be employed. A classical way to stabilize the high symmetry (cubic or tetragonal) phases is adding yttria at a level of several percent. The YSZ tetragonal phase has two structural variants: t′ (differing from the T by partial occupation of Zr sites by Y atoms), and, for large yttria content, t″ (as t′ phase, but with $c/a = 1$), differing by the details of their structure and by physical properties [14–16].

For ZrO_2 and for YSZ, due to close structural relationships, distinguishing of cubic and tetragonal (t′, t″) phases during the X-ray diffraction (XRD) based iden-

* corresponding author; e-mail: `ewerner@ifpan.edu.pl`

tification refinement process is not straightforward, as peaks from these phases overlap strongly. To distinguish between the high symmetry phases, the Raman spectroscopy and neutron diffraction can be useful [17]. As the overlap concerns the peak positions rather than intensities, this problem may be, in such cases, frequently solved by using the Rietveld method (an example are the results of Ortiz et al., for SiC polytypic mixture characterised by a strong overlap [18]).

In several recent papers, the Rietveld method was used to determine the phase relationships and lattice parameters for pure YSZ samples prepared with specific methods and having distinct crystallite size. Bokhimi et al. [1] have studied the formation of tetragonal and cubic nanocrystalline YSZ (up to 10 mol% yttria) from yttrium-doped hydrated zirconia. The studied material was synthesised by hydrolysis of the mixture of $ZrOCl_2 \cdot 8H_2O$, yttrium chloride and ammonium hydroxide. The phase composition strongly depended on the annealing conditions and yttria content. The size of the nanocrystals ranged from 8 nm (for cubic phase) to 17 nm (for tetragonal phase) and increased with the annealing temperature and decreased with increasing yttria content. Formation of YSZ was found for crystallization at 400 °C, whereas the process using 200 °C did not lead to crystallization. Lamas et al. [19, 20] have studied the structure of nanocrystalline powders of ZrO_2 with 3 to 12 mol% Y_2O_3. The material was synthesized by a nitrate-citrate gel-combustion process and it has been found that for all compositions the structure is tetragonal (t'/t'' boundary at 9 mol% of yttria), with c/a_f ratio decreasing towards unity with increasing Y_2O_3 content. The crystallite size was about 11 nm for the t' phase and about 8 nm for the t phase. Viazzi et al. [21] have studied the structure of metastable tetragonal YSZ powders produced via a sol–gel route. The samples were studied as a function of yttria content and annealing temperatures up to 1400 °C. The tetragonal (t') phase was obtained for the $YO_{1.5}$ content between 4.5 and 12 mol%, major content of $YO_{1.5}$ led to the higher symmetry phase — t'' or C. The grain sizes were less than 40 nm.

Among possible rare-earth zirconia dopants, praseodymium did not attract much attention in previous studies. Huang and Worcell [22] have studied the Pr doped YSZ using X-ray diffraction and extended X-ray absorption fine structure (EXAFS) techniques, determining, in particular, the influence of Pr doping of the structure type and on unit-cell size. These authors conluded that praseodymium ions in YSZ are in 3+ valence state. Suchorski et al. [23] have studied the effect of Pr doping on ZrO_2 on the phase composition and the distribution of Pr^{3+} in the nanocrystallites that have the core-shell-like structure. These authors have observed a stabilising effect of praseodymium on the tetragonal structure of zirconia and have concluded an enrichment of the surface region in Pr.

In this paper, the phase relationships and structural data are presented for Pr doped YSZ samples.

2. Experimental

Nanoscaled ZrO_2, ZrO_2:Pr^{3+} and yttria-stabilized YSZ:Pr^{3+} powders with compositions defined in Table I were obtained via a hydrothermal microwave driven process [24] at conditions described in detail in Ref. [5]. Obtained samples were dried at 70 °C during 24 h (unannealed samples) and then heated in air up to 1200 °C at a rate of 13 °C min^{-1} and held at the same temperature for 5 min (annealed samples). The annealed samples, after annealing, were freely cooled to room temperature.

TABLE I

The yttria and Pr_2O_3 content, and codes of the studied samples.

Y_2O_3 [mol%]	Pr_2O_3 [mol%]	Unannealed sample code	Annealed sample code
0.0	0.0	A1	A2
0.0	0.4	B1	B2
3.6	0.4	C1	C2
4.8	0.4	D1	D2
5.6	0.4	E1	E2
6.6	0.4	F1	F2
8.3	0.4	G1	–
11.1	0.4	H1	–

The powder samples were characterized by X-ray diffraction using a Philips X'pert MPD ALPHA PRO diffractometer operated at 40 kV and 30 mA with Cu K_{α_1} radiation and a primary-beam Johansson Ge monochromator and a strip detector. Data were collected in a continuous mode, and recorded with a step length of 0.0167° in the angular region of 2θ from 5° to 159°.

The changes in ZrO_2 structure and microstructure due to annealing, Pr^{3+} doping (≈ 0.4 mol%) and yttria (Y_2O_3) doping (0 mol%, 3.6 mol%, 4.8 mol%, 5.6 mol%, 6.6 mol%, 8.3 mol%, and 13.1 mol%) were studied. The Rietveld method performed with FullProf2k program [25] was used for quantitative phase analysis and structure refinement.

The yttrium atoms were assumed to partially occupy at Zr^{4+} sites in all, M, t' and C, structures, in the YSZ:Pr^{3+} samples (C1–H1, C2–F2), in the Rietveld analyses. The (Zr^{4+}, Y^{3+}) cations and O^{2-} anions were assumed: (i) at 4e position for the monoclinic phase, (ii) respectively at 2a and 4d positions for the tetragonal (t') phase, (iii) at 4a (Zr^{4+}, Y^{3+}) and 8c (O^{2-}) positions for the cubic phase. A pseudo-Voigt function was used to describe the peak shape. The number of fitted parameters depended on number of phases present in each diffraction pattern. Such parameters as: the lattice parameters, the atomic positions (with the exception of minority phases), scale, shape parameters (Shape, X), FWHM parameters (U, V, W), atomic displacement factors, were independently fitted for each component phase. A sample displacement parameter and asymmetry (four parameters

applied at angles below 65°) were fitted for all phases together. The background was satisfactorily fitted with a five- (unannealed samples) or six-parameter (annealed samples) polynomial function.

For the ZrO_2:Pr^{3+} samples ($B1$, $B2$) two models were used. In the first model, the praseodymium atoms were assumed to partially occupy the Zr^{4+} sites in all phases, whereas the second model neglected the presence of Pr. The difference between the fitting results of both models was insignificant. Consequently, the praseodymium contribution in the zirconia structure was ignored in the further analysis.

Various models were tested aiming for selection of the best-fitting phase composition, the models differed by the presence of C or t′ or both these phases.

3. Results

3.1. Selection of models

The models applied were built on the basis of phase identification. In case of doubt (similarity of peak positions among C, T, t′, t″ phases) the final model was selected on the basis of the best Bragg R-factor. The three phases' model (M, t′, C) was used for samples $C1$ and $D1$. The representative example of refinement for three-phase sample is shown in Fig. 1. The models with two phases were used for samples: (i) $A1$, $A2$, $B1$ and $B2$ — phases M and T, (ii) $E2$ and $F2$ — phases t′ and C. A model with C phase was used for samples $G1$ and $H1$. For selected samples two models were compared:
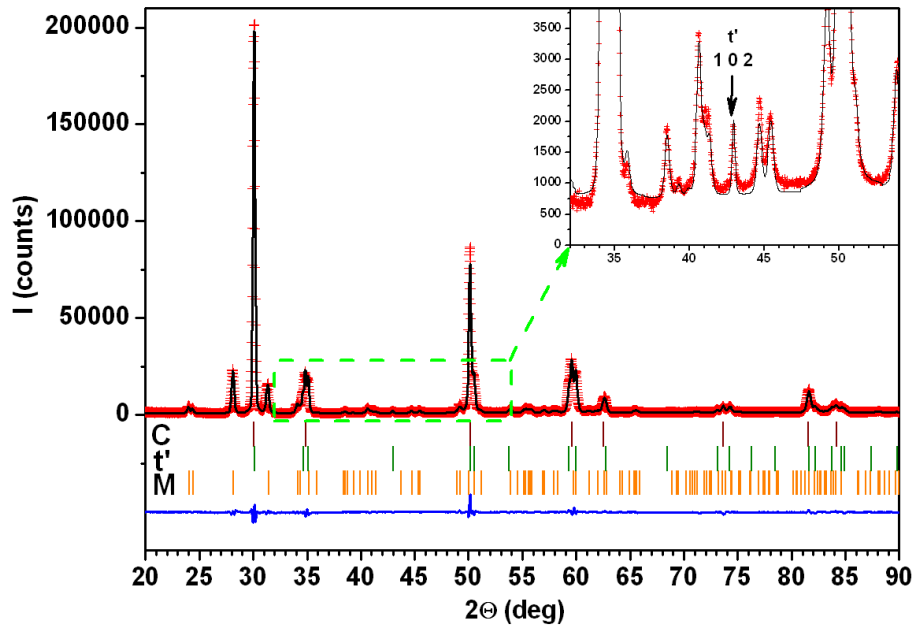

Fig. 1. (color on-line) Details of Rietveld refinement plot of the Pr-doped ZrO_2–Y_2O_3(4.8 mol%) after annealing at 1200 °C (sample $D2$). Experimental pattern is formed from crosses and the solid line is the calculated profile; vertical bars labeled C, t′ and M show the positions of diffraction peaks of the cubic, tetragonal and monoclinic phases, respectively. Difference patterns are shown below the bars. The inset documents the presence of tetragonal phase in the sample and the fit quality. The characteristic weak reflection of this phase, 102, is indicated by an arrow.

- for samples $C2$ and $D2$: (1) model with M and t′ phases, (2) model with M, t′ and C phases. The second model gave better results (Bragg R-factor for t′ and C phases ≈ 2, and for M phase ≈ 5) as compared to the first one (Bragg R-factor ≈ 10).

- for samples $E1$ and $F1$: (1) model with C and t′ phases, (2) model with single C phase. The second model fits better (Bragg R-factor ≈ 3–4) than the first one (Bragg R-factor ≈ 4–5).

However, owing to the above-mentioned similarity of the cubic and tetragonal structures causing that the Rietveld refinement is not sensitive enough, for the sam-

ples where two high-symmetry phases coexist, their relative content must be treated as indicative, only.

3.2. Phase composition

The addition of praseodymium to pure zirconia is found to cause a slight change of the phase content. In the sample doped with Pr^{3+} the content of the tetragonal phase is higher than in pure ZrO_2 (see Table II, Table III).

The addition of Y_2O_3 to ZrO_2:Pr^{3+} leads to increase of content of high-symmetry (C, t′) phases. In particular, in all samples with yttria addition exceeding 5.5 mol%, there is no trace of the monoclinic phase. In such sam-

TABLE II

Phases content (weight %) in unannealed samples.

Sample	M phase	T/t$'$ phase	C phase
A1	22.9(0.6)%	77.1(1.1)%	0%
B1	21.0(0.7)%	79.0(1.2)%	0%
C1	5(0.7)%	69(12)%	26(9)%
D1	5(1)%	66(22)%	29(18)%
E1	0%	0%	100(4)*%
F1	0%	0%	100(5)*%
G1	0%	0%	100(6)%
H1	0%	0%	100(6)%

*The alternative model indicates a small ($\sim 10\%$) contriution of t$'$ phase

TABLE III

Phases content (weight %) in annealed samples.

Sample	M phase	T/t$'$ phase	C phase
A2	99.5(2.0)%	0.5(0.2)%	0%
B2	99.8(2.5)%	1.2(0.2)%	0%
C2	33.6(0.9)%	45.6(1.5)%	20.8(1.5)%
D2	22.7(0.9)%	38.2(1.9)%	39.1(2.2)%
E2	0%	69(5)%	31(4)%
F2	0%	82(7)%	18(5)%

ples, after annealing, a tendency for t$'$ phase domination is observed (Table II, Table III).

3.3. Microstructure

The average crystallites size was determined by X-ray diffraction using the Scherrer equation. The grain size was calculated from selected reflections with 2Θ of about $30°$–$60°$. The calculated size of the nanocrystals (see Table IV) of series $A1$–$H1$ of the Pr doped ZrO_2–Y_2O_3 powder varies from 4.4 nm to 12.4 nm (phase sequence C→T/t$'$ →M), whereas for the series $A2$–$F2$ of annealed samples it is changing from 32 nm to 40.4 nm (phase sequence T/t$'$ →M). As expected, the C phase is built from the smallest crystallites.

In Fig. 2, the SEM observations of $B1$ and $B2$ samples are presented. The SEM observation shows that the grain sizes for unannealed samples are ≈ 10 nm, and for annealed samples ≈ 100 nm. This tendency is in agreement with the crystallites size calculated by the Scherrer equation.

3.4. Monoclinic phase

The lattice parameters for the monoclinic phase in unannealed samples with 4 mol% and 5 mol% yttria doping have large uncertainties, because it is the minority phase. In unannealed samples, the lattice parameters, a and c, of M phase decrease between yttria-free sample

TABLE IV

The grain size calculated using the Scherrer equation with the symbol of phase for which it was calculated.

Sample	Unannealed		Sample annealed	Annealed	
	Grain size [nm]	Phase		Grain size [nm]	Phase
A1	9.5(1)	M	A2	40.4(1)	M
	7.8(1)	T		32(1)	T*
B1	12.4(1)	M	B2	40.3(1)	M
	8.1(1)	t$'$		36(2)	t$'$*
C1	7.5(1)	t$'$#	C2	36(2)	t$'$#
D1	7.5(1)	t$'$#	D2	33(1)	t$'$#
E1	4.4(1)	C	E2	34(1)	t$'$#
F1	4.8(1)	C	F2	35(1)	t$'$#
G1	4.8(1)	C		–	
H1	4.5(1)	C		–	

* Minority phase.

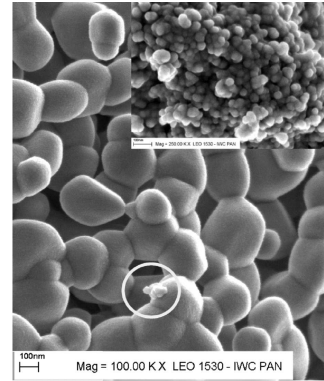# Calculated from 102 reflection with $2\Theta \approx 43.03°$.

Fig. 2. SEM observation of: the annealed ZrO_2:Pr^{3+} sample ($B2$) (the main picture) and the unannealed ZrO_2:Pr^{3+} sample ($B1$) (the inset). The majority phase of the $B1$ sample is the t$'$ phase with grain size of ≈ 10 nm. For sample $B2$, the M phase dominates, with grain size of ≈ 100 nm. The tetragonal crystallites (minority phase for the sample $B2$), smaller than the monoclinic ones, are shown in the circle at the main picture.

and 4 mol% of yttria (Table V). In annealed samples, the lattice parameters, a and c, of M phase rise between yttria-free sample and 4 mol% of yttria. Parameter b is constant in both series. These changes suggest that the solubility limit of yttria in the M phase as at the level of 4–5 mol% is achieved in both samples — 4 mol% and 5 mol% of yttria. The β angle decreases smoothly with rising Y_2O_3 content (Fig. 3). The angle change towards $90°$ correlates with a tendency of this system to adopt higher symmetries with Y_2O_3 doping. The refined β angles are comparable to the literature data for pure ZrO_2 [26] and for YSZ [1] (see Fig. 3).

TABLE V
The lattice parameters and volume for the monoclinic phase, their dependence from yttria content at the sample and the annealing temperature.

Sample code	a [Å]	b [Å]	c [Å]	β [°]	V [Å³]
			70 ℃		
$A1$	5.145(3)	5.209(3)	5.316(3)	99.30(4)	140.61(13)
$B1$	5.152(3)	5.210(3)	5.316(3)	99.41(3)	140.81(13)
$C1$	5.14(1)	5.21(2)	5.24(2)	98.8(2)	138.64(66)
$D1$	5.13(2)	5.21(2)	5.25(2)	98.6(3)	138.88(90)
			1200 ℃		
$A2$	5.1501(3)	5.2068(3)	5.3172(3)	99.228(4)	140.74(1)
$B2$	5.1490(4)	5.2110(4)	5.3159(4)	99.198(5)	140.80(2)
$C2$	5.1608(8)	5.2122(8)	5.3168(8)	99.094(9)	141.22(4)
$D2$	5.161(1)	5.208(2)	5.317(1)	99.06(2)	141.14(7)

The axial ratio calculated from those functions is presented as a solid line in Fig. 4. The difference between the present and literature in the slope of the line is attributed to the joint effect of Pr doping and difference in sample preparation way.

Fig. 4.   (color on-line) Variation of c/a with yttria content for tetragonal phase: unannealed YSZ:Pr³⁺ (●), pure, unannealed ZrO₂ (♦), YSZ:Pr³⁺ annealed at 1200 ℃ (▲), pure ZrO₂ annealed at 1200 ℃ (×). Comparison with literature: results of [1] (□), annealing at 800 ℃, results of [20] (◇) for sample treated at 350 ℃ and calcined at 600 ℃, and results of Viazzi et al. [21] (○) — sample annealed at 950 ℃. The axial ratio calculated from a function reported in Ref. [27] is presented as a straight solid line.

3.6. Cubic phase

The refined values of lattice parameter for cubic phase in unannealed and annealed samples are shown in Fig. 5.
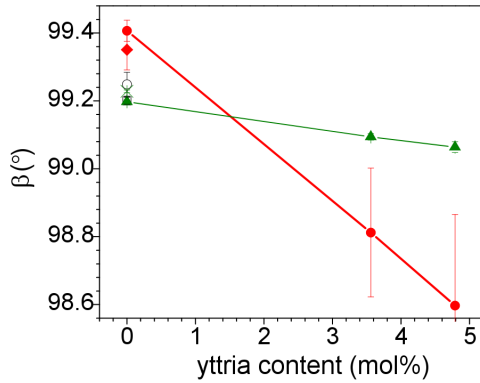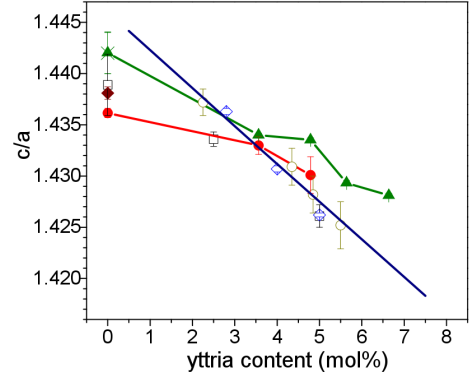

Fig. 3.   (color on-line) Dependence of β angle on yttria content for the monoclinic phase. The experimental points are presented as: for unannealed YSZ:Pr³⁺ (●), pure, unannealed ZrO₂ (♦), YSZ:Pr³⁺ annealed at 1200 ℃ (▲), pure ZrO₂ annealed at 1200 ℃ (×). The points from literature for pure ZrO₂ are presented for samples annealed at 800 ℃ reported in Ref. [1] (□), and in Ref. [26] (○).

3.5. Tetragonal phase

For both sample sets (treated at 70 ℃ and 1200 ℃) the lattice parameters of the t′ phase vary with yttria content, giving a clear decrease of axial ratio (c/a) by $\approx 0.7\%$ (see Table VI). The increase of Y₂O₃ content, in the annealed samples, gives a small increase of unit cell volume by about 0.7%. In the unannealed samples (70 ℃) the unit cell volume rise with yttria content is weaker.

The slope of the c/a dependence on yttria content is similar for annealed and unannealed samples, and it is consistent with literature data (see Fig. 4). Viazzi et al. [21] showed, after Ref. [27], the lattice parameters for the tetragonal (t′) phase, as functions of yttria content (YO$_{1.5}$ in mol%) x:

$$a\sqrt{2}\ [\text{Å}] = 5.0801 + 0.3582x, \tag{1}$$

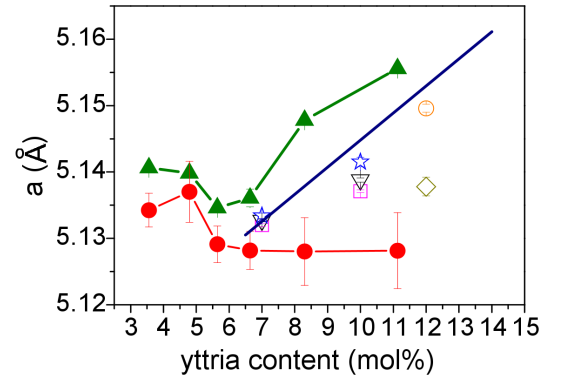$$c\ [\text{Å}] = 5.1944 - 0.3045x. \tag{2}$$

Fig. 5.   (color on-line) Variation of YSZ lattice parameter, a, with yttria content for cubic phase: unannealed YSZ:Pr³⁺ (●), YSZ:Pr³⁺ annealed at 1200 ℃ (▲). Comparison with literature: (i) results of Bokhimi et al. [1]: sample annealed at 800 ℃ (□), at 600 ℃ (▽), and at 400 ℃ (⋆), (ii) results of Ref. [20] (◇), sample treated at 350 ℃ and calcined at 600 ℃, and (iii) results of Lamas et al. [19] (○) — annealed at 1000 ℃. The lattice parameter function by Scott [27] for undoped YSZ, is presented as a solid line.

TABLE VI

The lattice parameters for the tetragonal phase, their dependence on yttria content at the sample and on annealing.

Sample	Unannealed			Sample	Annealed		
	a [Å]	c [Å]	V [Å^3]		a [Å]	c [Å]	V [Å^3]
A1	3.5984(5)	5.174(1)	67.00(2)	A2	3.595(3)	5.184(7)	67.0(1)
B1	3.6008(6)	5.171(1)	67.05(3)	B2	3.598(3)	5.188(6)	67.2(1)
C1	3.605(1)	5.166(3)	67.13(5)	C2	3.6085(2)	5.1746(4)	67.38(1)
D1	3.607(2)	5.158(6)	67.09(9)	D2	3.6087(3)	5.1731(6)	67.37(1)
E1				E2	3.6138(4)	5.1654(6)	67.46(1)
F1				F2	3.6160(3)	5.1640(6)	67.52(1)

Interestingly, there is a difference between the lattice parameter behavior for annealed and unannealed samples. For unannealed ones a is constant, for annealed ones an increase is observed. The less regular behavior at low yttria content region is attributed to difficulties in analysis of multiphase material. The results are compared with available literature points [1, 19, 20] for annealed YSZ, as well as the linear dependence reported by Scott [27] for undoped YSZ (a [Å] = 5.104 + 0.204x; x representing $YO_{1.5}$ content in mol%, for $0.18 < x < 0.90$). This function is presented as a solid line in Fig. 5. The literature data also show increasing tendencies with rising yttria content. The variations of the a with yttria content differ among the data, showing that the slope may vary depending on the sample preparation route (e.g. on the annealing conditions).

It is noteworthy that the occurrence of another metastable tetragonal phase, called t″, has been revealed by the Raman spectroscopy and neutron scattering for YSZ [15, 17]. The difference between t″ phase and C phase is only in the oxygen displacement from its position in the fluorite unit cell.

The tetragonal (t″) phase cannot be distinguished from cubic phase by X-ray diffraction analysis. Because of that, in the Rietveld analysis, the model with cubic phase (without t″) was used after checking that using the t″ based models does not improve the Bragg R-factor.

4. Conclusions

ZrO_2–Y_2O_3:Pr^{3+} samples, prepared via a hydrothermal microwave driven process, with varying heat treatment and composition are characterized. Similarities and differences observed in respect of the literature data for undoped YSZ are discussed. The annealing process leads to partial or full transformation of the high symmetry phases to monoclinic phase. In the annealing process the grain size increases. It causes variations of lattice parameters for all component phases. The lattice parameter for cubic phase increases and the axial ratio at tetragonal phase decreases with yttria doping. The difference between the presented results and literature ones,

in the slope of the lines, is attributed to the joint effect of Pr doping and difference in sample preparation way. Due to yttria doping, the β angle of the monoclinic phase decreases towards 90°.

References

[1] X. Bokhimi, A. Morales, A. Garcia-Ruiz, T.D. Xiao, H. Chen, P.R. Strutt, *J. Solid State Chem.* **142**, 409 (1999).

[2] J.P. Feist, A.L. Heyes, *Proc. Inst. Mech. Eng., Part L, J. Mater., Des. Appl.* **214**, 7 (2000).

[3] S. Gutzov, W. Assmus, *J. Mater. Sci. Lett.* **19**, 275 (2000).

[4] X. Fu, S. Niu, H. Zhang, Q. Xin, *Mater. Sci. Eng. B* **129**, 14 (2006).

[5] J.D. Fidelus, S. Yatsunenko, M. Godlewski, W. Paszkowicz, E. Werner-Malento, W. Łojkowski, *Scr. Mater.* **61**, 415 (2009).

[6] M. Godlewski, M. Leskelä, *CRC Crit. Rev. Solid State Mater. Sci.* **19**, 199 (1994).

[7] M. Godlewski, S. Yatsunenko, M. Zalewska, A. Kłonkowski, T. Strachowski, W. Łojkowski, *Solid State Phenom.* **128**, 123 (2007).

[8] M. Godlewski, S. Yatsunenko, A. Nadolska, A. Opalińska, W. Łojkowski, K. Drozdowicz-Tomsia, E.M. Goldys, *Opt. Mater.* **31**, 490 (2009).

[9] D.K. Smith, H.W. Newkirk, *Acta Crystallogr.* **18**, 983 (1965).

[10] G. Teufer, *Acta Crystallogr.* **15**, 1187 (1962).

[11] R.W.G. Wyckoff, *Crystal Structures*, 2nd ed., Vol. 1, Wiley, New York 1963.

[12] O. Ohtaka, D. Andrault, P. Bouvier, E. Schultz, M. Mezouar, *J. Appl. Crystallogr.* **38**, 727 (2005).

[13] J. Ciosek, W. Paszkowicz, P. Pankowski, J. Firak, U. Stanislawek, Z. Patron, *Vacuum* **72**, 135 (2004).

[14] M. Yashima, N. Ishizawa, M. Yoshimura, in: *Proc. Int. Conf. on Zirconia V*, Eds. S.P.S. Badwal, M.J. Bannister, R.H.J. Hannink, Technomic, Lancaster, PA 1993, p. 125.

[15] M. Yashima, N. Ishizawa, M. Yoshimura, *J. Am. Ceram. Soc.* **76**, 641 (1993).

[16] M. Yashima, M. Kakihana, M. Yoshimura, *Solid State Ionics* **86-88**, 1131 (1996).

[17] M. Yashima, K. Ohtake, H. Arashi, M. Kakihana, M. Yoshimura, *J. Appl. Phys.* **74**, 7603 (1993).

[18] A.L. Ortiz, F.L. Cumbrera, F. Sánchez-Bajo, F. Guiberteau, H. Xu, N.P. Padture, *J. Am. Ceram. Soc.* **83**, 2282 (2000).

[19] D.G. Lamas, N.E. Walsöe de Reca, *Mater. Lett.* **41**, 204 (1999).

[20] D.G. Lamas, N.E. Walsöe de Reca, *J. Mater. Sci.* **35**, 5563 (2000).

[21] C. Viazzi, J.-P. Bonino, F. Ansart, A. Barnabé, *J. Alloys Compd.* **452**, 377 (2008).

[22] J.Q. Huang, W.L. Worcell, in: *High-temperature Materials from 201st Meeting of the Electrochemical Society, Philadelphia 2002, ECS. Proc.*, Vol. 2002–5, Ed. S.C. Singhal, Electrochemical Society, Pennington, NJ 2002.

[23] Y. Suchorski, R. Wrobel, S. Becker, A. Opalińska, U. Narkiewicz, M. Podsiadly, H. Weiss, *Acta Phys. Pol. A* **114**, S125 (2008).

[24] A. Opalińska, C. Leonelli, W. Łojkowski, R. Pielaszek, E. Grzanka, T. Chudoba, H. Matysiak, T. Wejrzanowski, K.J. Kurzydłowski, *J. Nanomater.* **98769**, 1 (2006).

[25] J. Rodriguez-Carvajal, *Physica B* **192**, 55 (1993).

[26] *Inorganic Crystal Structure Database* #172161, Karlsruhe 2009, 2007/04/01.

[27] H.G. Scott, *J. Mater. Sci.* **10**, 1527 (1975).